Energy, Environmental, and Catalysis Applications

High-Performance Thermoelectric Generators for Field Deployments

Ravi Anant Kishore, Amin Nozariasbmarz, Bed Poudel, and Shashank Priya

ACS Appl. Mater. Interfaces, **Just Accepted Manuscript** • DOI: 10.1021/acsami.9b21299 • Publication Date (Web): 10 Feb 2020

High-Performance Thermoelectric Generators for Field Deployments

Ravi Anant Kishore, [*a b +] Amin Nozariasbmarz, [c +] Bed Poudel, [c] and Shashank Priya [*a c]

[a.] Center for Energy Harvesting Materials and Systems, Virginia Tech, Blacksburg, VA 24061, USA.

[b.] National Renewable Energy Laboratory, 15013 Denver West Pkwy, Golden, CO 80401, USA.

[c.] Department of Materials Science and Engineering, Pennsylvania State University, University Park, PA 16802, USA.

[*] Corresponding authors: Ravi Anant Kishore (ravi86@vt.edu), Shashank Priya (sup103@psu.edu)

[+] These authors contributed equally to this work.

Abstract

Thermoelectric power generation is a reliable energy harvesting technique for directly converting heat into electricity. Recent studies have reported the thermal-to-electrical energy conversion efficiency of thermoelectric generators (TEGs) up to 11% under laboratory settings. However, the practical efficiency of TEGs deployed under real environment is still not more than a few percent. In this study, we provide fundamental insight on the operation of TEGs in realistic environments by illustrating the combinatory effect of thermoelectric material properties, device boundary conditions, and environmental thermal resistivity on TEG performance in conjunction with the module parameters. Using numerical and experimental studies, we demonstrate the existence of a critical heat transfer coefficient that dramatically affects the design and performance of TEGs. This provides a set of concrete design criteria for designing efficient TEGs that meet the metrics for field deployments. High-performance TEGs demonstrated in this study generated up to 28% higher power and 162% higher power per unit mass of thermoelectric materials as compared to the commercial module deployed for low-grade waste heat recovery. This advancement in understanding the TEG operation will have a transformative impact on the development of scalable thermal energy harvesters and in realizing their practical targets for efficiency, power density and total output power.

Keywords: Thermoelectric; TEG; deployment; optimization; heat flux; field test.

Introduction

Thermoelectric generators (TEGs) offer a promising clean energy solution for generating electricity from heat. [1-2] As shown in Figure 1(a), TEGs are solid-state devices comprising of p- and n- type thermoelectric (TE) legs connected electrically in series and thermally in parallel. When a temperature difference is applied across the two sides of a TEG, electrons in n-type and holes in p-type legs flow from hot-side to cold-side causing an electric current, termed as thermoelectricity (Figure 1(b)). TEGs have no moving parts, require no working fluid, involve no chemical reactions, and produce no emissions. [3-4] They are noiseless, reliable, light-weight, and scalable, making them ideal for power generation from distributed thermal energy sources, [5-6] such as waste heat [7] or natural heat [8]. In past few decades, TEGs have received tremendous attention from researchers as well as industry. The global TEG market was reported to be nearly $250 million in 2016 and is expected to grow over $550 million by 2022. [9] The wide range of TEG applications include cogeneration [10-11] in power plants, waste heat recovery [11-14] in automotive and aerospace industries, energy harvesting [15-17] for self-powered sensors and wearables, and direct power generation [8, 18-20] from solar and geothermal heat. However, compared to traditional heat engines in large-scale applications, TEGs exhibit lower efficiency. [21] One of the main reasons for this lower performance is low figure-of-merit (zT) of the TE materials. The state-of-the-art quantum dot TE materials exhibit $zT > 2.0$, but they are prohibitively expensive and not practical for commercial power generation applications.[21] The zT for commercial TE materials is close to unity. [22] The device level figure-of-merit, usually denoted by ZT (with upper case Z), has been reported to be at least 30-50% lower than the material zT, [6, 23-24] which indicates a very strong influence of the module configuration on the TEG performance. Considerable research efforts have been made to improve zT of existing TE materials and discover new classes of TE materials having high zT. [6] However, there still exists a broad technological gap between the material and device performance.[24] Inappropriate material selection, poor module design and unrealistic characterization methods may result in significant drop in TEG performance under practical conditions in comparison to the expected laboratory results.

Figure 1(c) illustrates the schematic of experimental set-up currently used to characterize TEG modules in laboratory. In laboratory settings, TEG experiments are typically performed under constant temperature boundary condition, where temperature on hot- and cold-sides of the module is fixed at certain value. The constant temperature boundary condition, however, is an ideality that

assumes an infinite capacity heat source which remains unperturbed by the heat drawn through the TEG. In practice, however, TEGs are mostly deployed on a source that generates heat at a certain rate. Therefore, in practical situations, TEGs are more likely to experience constant heat flux boundary condition as compared to constant temperature boundary condition (Figure 1(d)). In addition, unlike the constant temperature heat source, the real heat source/sink has a finite heat capacity and thermal resistance (Figure 1(e)). The actual heat source/sink is affected by TEG deployment and consequently the hot- and cold-side temperatures of TEG do not remain equal to the core temperature of the heat source/sink. The change in the boundary condition and the external thermal resistance has strong influence on the TEG performance and consequently the TEG designed in the laboratory settings do not perform optimally during real field deployments. Rather a substantial drop in the efficiency is observed. As shown in Fig 1(f), the system-level efficiency for waste heat recovery using TEGs has been reported to be 30-60% lower than the module-level efficiency. [25-26]

A significant amount of effort has been made in the past to optimize TEG geometry, such as leg length, leg cross-sectional area, and the number of leg pairs. [27-31] While most studies have used absolute dimensions in their analysis, some researchers have suggested using non-dimensional parameters such as fill fraction [32], aspect ratio [33], slenderness ratio [34], and other shape parameter [35], which are essential for scaling-up thermoelectric power for sizable application. Evaluating the influence of numerous parameters that affect TEG performance requires rigorous time-consuming experimentation; therefore TEG optimization is often corroborated by analytical and numerical modelling, which can either be simplified one-dimensional model [36-37] or complex three-dimensional model. [38-41] One-dimensional models are easy to implement and provides fairly accurate results (error up to 10% [42-43]) when thermal gradient is small, material properties are temperature-independent, and contact resistances are insignificant. [22] However, for more robust analysis, three-dimensional model is preferred to account for temperature dependent material properties and various kinds of losses. [44-45] Although majority of the modeling studies in the past have replicated the TEG operation under laboratory settings and focused primarily on optimizing the internal parameters of TEGs, few researchers have attempted to understand the TEG operation at system-level and noted significant deviation in TEG characteristics from the ideal performance. For instance, studies on TEGs for waste heat recovery have shown strong influence of heat exchanger parameters such as channel width, channel height, fin type, fin density and fin thickness

along with convection, conductive, and contact thermal resistances. [46-47] TEG performance for body energy harvesting has been found to be dictated by internal thermal resistance, which must be high and comparable to the parasitic thermal resistances in series with the TEG. [48-51] Thermal resistance/ impedance matching studies have shown that maximum TEG power is obtained when the temperature drop across the module is nearly equal to half of the temperature difference between heat source and heat sink. [52-53] Systematic assessment of TEG for solar energy harvesting and other radiant heat recovery systems requires different analytical approach than the traditional modeling, where TEGs are usually subjected to a constant temperature condition. Under the constant heat flux condition, the hot-side temperature is not fixed but depends on the inward heat flux and the heat transfer capacity at the cold-side. [54-56].

While most of TEG studies in the past have been focused on a specific application, we aim to provide a comprehensive assessment including the TE material characteristics, the TEG module design and the device characterization method to achieve enhanced TEG performance for practical applications. In this study, we provide fundamental insight on TEGs deployed in different realistic environments and reveal that the currently designed TEGs (such as commercial TEG modules) may not fit for all practical scenarios. We have attempted to bridge the gap between the thermoelectric phenomena occurring at the material and device levels by illustrating the combinatory effect of TE material properties, device boundary conditions, and operating environments on TEG performance in conjunction with TEG design. Most importantly, using numerical and experimental studies, we demonstrate the occurrence of a critical heat transfer coefficient that greatly affects the design and performance of TEG modules. Lastly, we fabricated TEG modules of different fill fractions varying from 36% to as low as 1.7% and deployed them on a hot-water pipe for low-grade waste heat recovery to compare their performance versus power generation by commercial TEG modules. We note that our optimized TEG generates 28% higher power and 162% higher power density per unit mass of the TE materials than the commercial module.

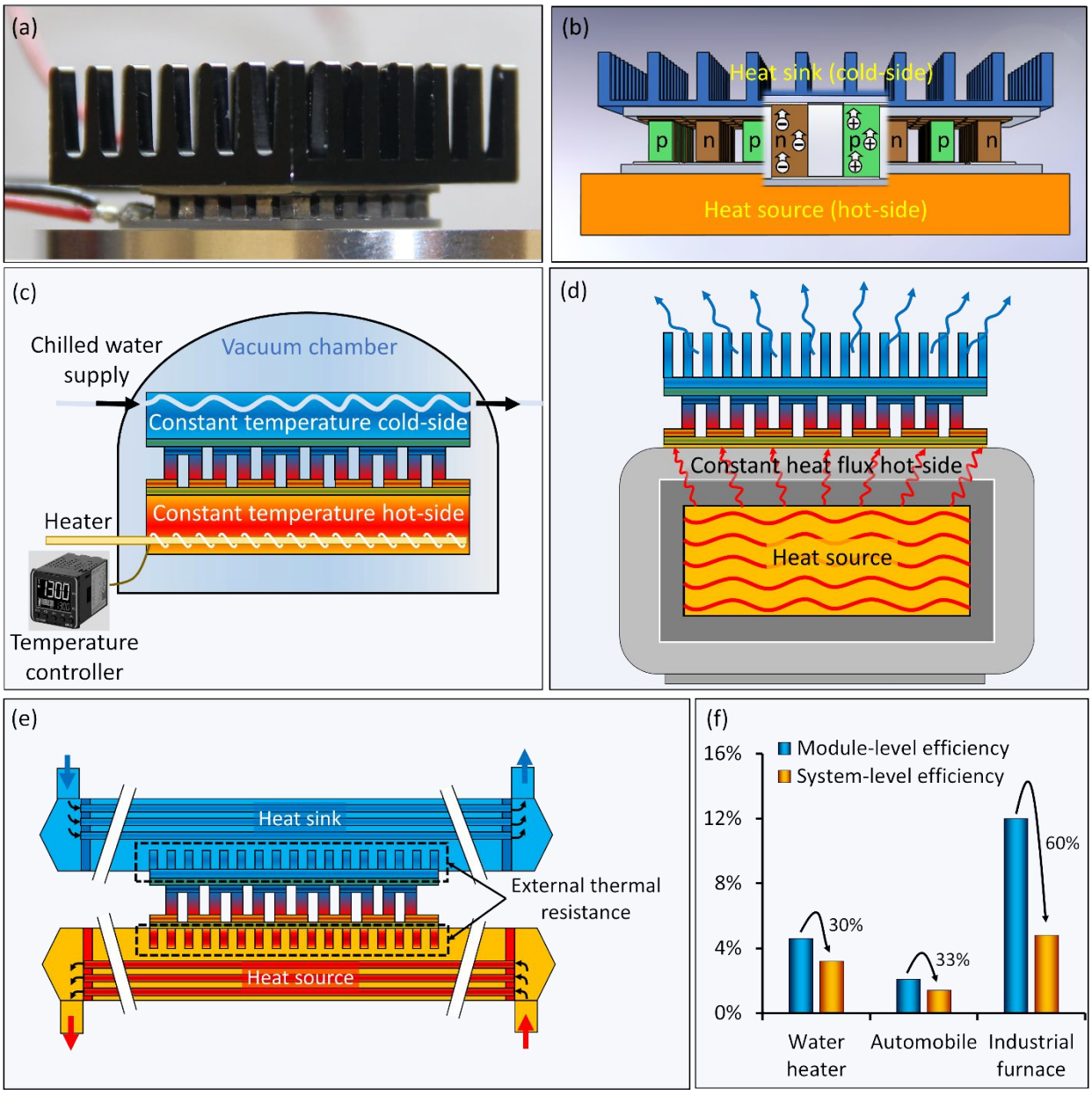

Figure 1. (a) A thermoelctric generator (TEG) placed between a heat source and a heat sink. TEGs consist of multiple p- and n-type thermoelectric legs, connected electrically in series and thermally in parallel. (b) The temperature difference across the two sides of TEG causes electrons in n-type and holes in p-type legs to flow from hot-side to cold-side causing an electric current, termed as thermoelectricity. (c) Schematic of TEG characterization in a laboratory setup. TEGs are typically tested under the constant temperature boundary conditions, where temperature on hot- and cold-sides are maintained at specific value. (d) Schematic illustration of TEG operation during a practical deployement. In practical scenarios, TEGs are usually attached to a heat source that

generates heat at a certain rate. (e) Schematic of a realistic boundary conditions during the practical deployment of TEGs. Unlike constant temperature heat source/sink, the real heat source/sink has a finite heat capacity and certain thermal resistance. (f) Difference in the module- and system-level efficiencies for waste heat recovery using TEGs. System-level efficiency has been reported to be 30-60% lower than the module-level efficiency (information taken from [25-26]).

Results and discussion

The effect of boundary conditions on TE material behavior

The thermal-to-electrical energy conversion efficiency of a TE material is theoretically dependent on three key material parameters: Seebeck coefficient (S), electrical conductivity (σ), and thermal conductivity (κ), which are collectively expressed in terms of a dimensionless figure-of-merit (zT) as[23, 57-59]

$$zT = \frac{S^2\sigma}{\kappa}T, \quad (1)$$

where T is the absolute temperature of the TE material at the point of measurement.

The change of boundary conditions affects the heat flow and thus the temperature distribution in the TEG module. Since the TE material properties are strongly temperature dependent, change in boundary conditions dramatically affects the material behavior and thus the TEG performance. In order to understand this effect, various TEG modules were modeled in this study. Table 1 illustrates the key features of these TEG modules.

Table 1. The key geometric dimensions and features of the TEG modules

Description	
Leg height	1.6 mm
Leg base area	1.6 × 1.6 mm^2
Fill fraction	25%
Electrical contact resistivity	10^{-9} Ω-m^2

Electrode material	Cu
Electrode thickness	0.2 mm
Substrate material	AlN
Hot-side temperature	200°C
Hot-side heat flux	1.0 W/cm^2
Cold-side temperature	22°C
Ambient temperature	22°C
Radiation emissivity for leg surfaces	0.45
Radiation emissivity for copper surfaces	0.03

The performance of TEG modules was evaluated under constant temperature and constant heat flux boundary conditions. The results are illustrated in Figure 2 using three-dimensional (3-D) plots. On the left-hand side, column (i) shows the plots for constant temperature boundary condition, whereas on the right-hand side, column (ii) depicts plots for constant heat flux boundary condition. Vertical axis of the 3-D plots shows the TEG performance parameters: (a) power under the optimal load, (b) efficiency under the optimal load, (c) voltage across the optimal load, and (d) temperature difference across the two sides of TEG under the optimal load. Horizontal axes of the 3-D plots contain Seebeck coefficient and thermal conductivity. The constant zT of 0.5 and 1.0 was maintained by systematically varying thermal conductivity and Seebeck coefficient while calculating electrical conductivity to keep the zT constant. It is evident from Figure 2 that TEG performances are drastically different under the two boundary conditions. Under constant temperature boundary condition (Figure 2(a-i)), Seebeck coefficient as well as thermal conductivity has a strong influence on TEG power. TEG power increases with increase in Seebeck coefficient as well as thermal conductivity. In contrast, under constant heat flux boundary condition (Figure 2(a-ii)), TEG power increases marginally with increase in Seebeck coefficient, but it increases dramatically with decrease in thermal conductivity. Most interestingly, under constant heat flux boundary condition, TE material having $zT = 0.5$ with low thermal conductivity (e.g. $\kappa = 0.5$ W/m^2-K) produces higher power than the TE material having $zT = 1.0$ with high thermal conductivity (e.g. $\kappa = 1.5$ W/m^2-K). The boundary conditions also alter the influence of material properties on TEG efficiency, as illustrated in Figure 2(b). Under constant temperature boundary condition (Figure 2(b-i)), efficiency initially increases with increase in

Seebeck coefficient, but it soon saturates to a maximum value. Thermal conductivity has negative impact on efficiency as efficiency slowly decreases with increase in thermal conductivity. On the other hand, under constant heat flux boundary condition (Figure 2(b-ii)), efficiency follows similar trend as power. TEG efficiency increases minimally with increase in Seebeck coefficient but it increases dramatically with decrease in thermal conductivity. Again, TE material having $zT = 0.5$ with low thermal conductivity (e.g. $\kappa = 0.5$ W/m^2-K) results in higher efficiency than the TE material having $zT = 1.0$ with high thermal conductivity (e.g. $\kappa = 1.5$ W/m^2-K). It is important to note that these observations are quite contradictory to the common perception about zT. It is usually perceived that high zT TE material provides high TEG efficiency. As we noted, high zT material certainly results in high efficiency when TEG is deployed under constant temperature boundary condition; however, this is not necessarily true when TEG is deployed under constant heat flux boundary condition.

The variation in TEG power and efficiency with change in TE material properties can be explained with the help of Figure 2(c) and (d) that depict the voltage difference across the optimal resistive load and the temperature difference across the two sides of TEG module. Under constant temperature boundary condition, output voltage is solely dependent on Seebeck coefficient and it increases linearly with increase in Seebeck coefficient (Figure 2(c-i)). The temperature difference does not change in this case as temperature on the two sides of TEG is fixed (Figure 2(d-i)). On the contrary, under constant heat flux boundary condition, the voltage and temperature difference follow the same trend as power and efficiency, indicating a close relationship between temperature difference and TEG performance (Figure 2(c-ii) and 2(d-ii)). Using the simplified one-dimensional model, the load voltage (V_{opt}), TEG power (P_{opt}), and maximum efficiency (η_{max}) under the optimal load ($R_L = R_{eTEG}\sqrt{1+Z\bar{T}}$) are expressed as (refer Supporting Information for the derivations)

$$V_{opt} = nS(T_h - T_c)\frac{\sqrt{1+Z\bar{T}}}{1+\sqrt{1+Z\bar{T}}} \quad (2)$$

$$P_{opt} = \frac{(nS(T_h - T_c))^2}{R_{eTEG}}\frac{\sqrt{1+Z\bar{T}}}{(1+\sqrt{1+Z\bar{T}})^2} \quad (3)$$

$$\eta_{max} = \frac{P_{opt}}{Q_h} = \frac{(T_h - T_c)}{T_h}\left[\frac{\sqrt{1+Z\bar{T}} - 1}{\sqrt{1+Z\bar{T}} + \frac{T_c}{T_h}}\right] \quad (4)$$

where $Z\overline{T}$ is the TEG module figure-of-merit at mean temperature $\overline{T} = {(T_h + T_c)}/{2}$ and it is given as [22, 60]

$$Z\overline{T} = \frac{S^2}{R_{eTEG}} R_{tTEG} \overline{T} \quad (5)$$

where T_h and T_c are hot- and cold-side temperatures, and R_{eTEG} and R_{tTEG} are the module internal electrical and thermal resistances.

It should be noted that the one-dimensional model given above is just to explain the physics and observations. For the results shown in the paper, we have used the three-dimensional equations of thermoelectricity in steady state, which are described in Supporting Information. Observing equations (2)-(4), we can note that increasing Seebeck coefficient (S) increases power and voltage, which is visible in Figure 2(a) and (c) for both the boundary conditions. Also, increasing thermal conductivity (κ) decreases TEG thermal resistance (R_{tTEG}), which tends to reduce temperature difference ($T_h - T_c$), if T_h and T_c are allowed to vary. In the case of constant temperature boundary condition, T_h and T_c are fixed; therefore, varying κ has no effect on voltage (Figure 2(c-i)). However, in the case of constant heat flux boundary condition, increase in κ decreases temperature difference that eventually leads to reduction in TEG voltage (Figure 2(c-ii)). TEG power is directly proportional to $T_h - T_c$ but inversely proportional to module internal electrical resistance (R_{eTEG}). When zT and Seebeck coefficient are held constant, we can note using equation (1) that increase in κ leads to increase in electrical conductivity (σ), which ultimately reduces R_{eTEG}. Reduction in R_{eTEG} decreases Joule heating, and thus it has positive impact on TEG power. Under constant temperature boundary condition, therefore, power increases with increase in thermal conductivity (Figure 2(a-i)). Under constant heat flux boundary condition, however, reduction in $T_h - T_c$ with increase in κ appears to be very prominent (as noted in Figure 2(d-ii)). In this case, therefore, power decreases with increase in thermal conductivity (Figure 2(a-ii)). Lastly, using equation (4), we can note that efficiency is proportional to hot- and cold-side temperatures (T_h and T_c) and the device figure-of-merit ($Z\overline{T}$). Under constant temperature boundary condition, since temperatures are fixed, the maximum efficiency varies with variation in material properties (Figure 2(b-i)). Also, since $Z\overline{T}$ is proportional to square of S, Seebeck coefficient exhibits a strong influence on efficiency, which is evident in Figure 2(b-i). Under constant heat flux boundary condition,

however, since heat in-flow (Q_h) is fixed, efficiency is directly proportional to power and thus both these parameters exhibit similar trend (Figure 2(a-ii) and 2(b-ii)).

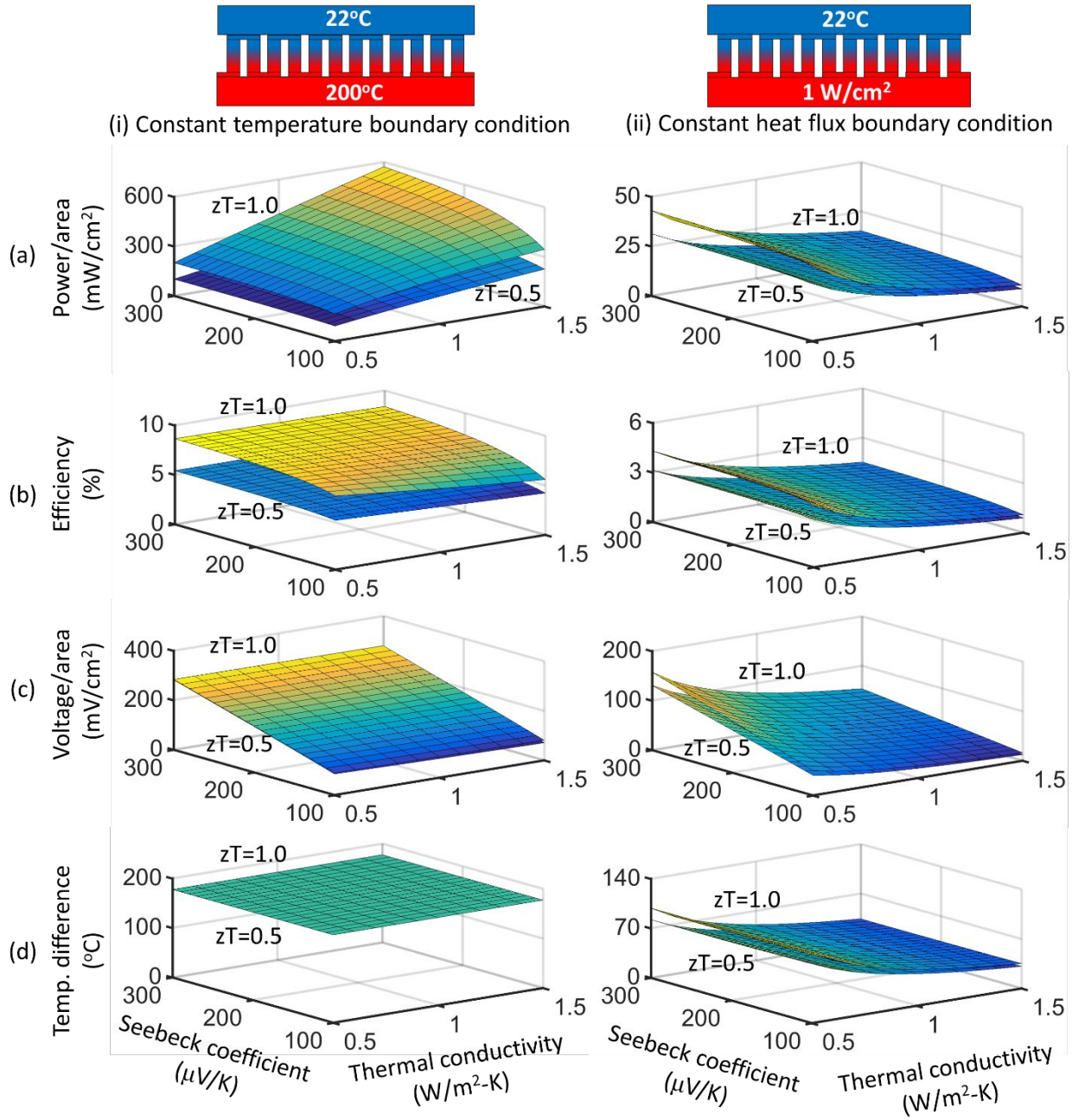

Figure 2. The combined effect of boundary conditions and material properties on TEG performance. TEG performance has been compared for TE materials having a constant zT of 0.5 and 1.0. Thermal conductivity and Seebeck coefficient are varied while electrical conductivity is

calculated to keep the zT constant. (a-i) Under constant temperature boundary condition, TEG power increases with increase in Seebeck coefficient as well as thermal conductivity. (a-ii) Under constant heat flux boundary condition, TEG power increases minimally with increase in Seebeck coefficient, but it increases drastically with decrease in thermal conductivity. (b-i) Under constant temperature boundary condition, TEG efficiency initially increases with increase in Seebeck coefficient but it soon saturates. Thermal conductivity has minor effect on efficiency. (b-ii) Under constant heat flux boundary condition, TEG efficiency increases minimally with increase in Seebeck coefficient, but it increases drastically with decrease in thermal conductivity. (c-i) Under constant temperature boundary condition, output voltage across the optimal load is solely dependent on Seebeck coefficient and it increases linearly with increase in Seebeck coefficient. (c-ii) Under constant heat flux condition, large Seebeck coefficient and small thermal conductivity result in high voltage. (d-i) Under constant temperature boundary condition, internal temperature difference ($T_h - T_c$) does not change with change in material properties. (d-ii) Under constant heat flux boundary condition, temperature difference follows the similar trend as the variation in power, efficiency, and voltage. Temperature difference is large when thermal conductivity is small, which leads to higher power and efficiency under constant heat flux boundary condition.

The effect of boundary conditions on module design

TEG design parameters consist of leg cross-sectional area, leg height, and number of legs, which are traditionally expressed in terms of two dimensionless parameters: fill fraction (FF) and leg aspect ratio (AR). FF is defined as the ratio of cross-sectional area occupied by the TE legs over the total TEG base area and leg AR is defined as the ratio of leg height (x) over leg cross-sectional width (w).

$$FF = 2n\frac{w^2}{A} \quad (6)$$

$$AR = \frac{x}{w} \quad (7)$$

where n is the number of leg pairs in the TEG module and A is the module base area. TEG design strongly affects the internal electrical resistance (R_{eTEG}) and thermal resistance (R_{tTEG}) of the TEG module, which are given as [60]

$$R_{eTEG} = n\frac{x}{a}\left(\frac{1}{\sigma_p} + \frac{1}{\sigma_n}\right) = 2n^2\frac{wAR}{A\,FF}\left(\frac{1}{\sigma_p} + \frac{1}{\sigma_n}\right) \quad (8)$$

$$R_{tTEG} = \frac{1x \quad 1}{na(\kappa_p + \kappa_p)} = 2\frac{wAR \quad 1}{A\,FF(\kappa_p + \kappa_p)} \quad (9)$$

where a is the leg cross-sectional area, σ_p and σ_n are electrical conductivity and κ_p and κ_p are thermal conductivity of p- and n-type materials.

Varying the TEG design in conjunction with boundary conditions dramatically influences the heat flow and temperature distribution in the TEG, which eventually affects the TEG performance. Figure 3 illustrates the effect of FF and AR on TEG performance under the two boundary conditions. The TEG models considered in this section utilize commercial p- and n-type bismuth telluride materials, whose temperature-dependent material properties are provided in Supporting information (SI Figure S2 and Figure S3). Other module parameters are as given in Table 1. It can be observed from Figure 3(a-i), that under constant temperature boundary condition, power under the optimal load increases almost linearly with increase in FF, whereas it decreases with increase in AR. This indicates that high FF and low AR provide high power when TEG is deployed under constant temperature boundary condition. In contrast, under constant heat flux boundary condition (Figure 3(a-ii)), TEG power decreases with increase in FF. In addition, there exists an optimal AR for each FF where TEG power is maximum. The optimal AR decreases with decrease in FF. For instance, when FF=25%, the optimal AR is close to 5.5, whereas when FF=10%, the optimal AR is around 2.5. It is quite interesting to note that the optimal TEG design (high FF and low AR) obtained for constant temperature boundary condition results in very low power under constant heat flux condition. This highlights an important observation as the TEG optimized in laboratory conditions (where boundary condition is usually fixed at constant temperature) performs very poorly in the practical conditions (where boundary condition is usually constant heat flux). The commercial modules usually have large FF (> 25%) and low AR (1.0-1.5). Clearly, these modules are not suitable for the applications where source generates heat at certain rate (constant heat flux condition).

Figure 3(b) shows variation in TEG efficiency with change in FF and leg AR. It can be noted from Figure 3(b-i) that under constant temperature boundary condition, TEG efficiency is not strongly influenced by changes in FF and AR; however, it is highest when AR is close to 1.5. On the other hand, under constant heat flux boundary condition (Figure 3(b-ii)), TEG efficiency follows similar

trend as the power. TEG efficiency is high at low FF and at an optimized AR. The optimum value of AR decreases with decrease in FF. The optimal AR needed for maximum efficiency is almost the same as that required for maximum power. Clearly, the TEG design required to maximize efficiency is different for the two different boundary conditions. This also indicates that commercial TEGs having FF ~ 25% and AR ~ 1.0-1.5 provide maximum efficiency under constant temperature boundary condition, but they perform poorly under constant heat flux boundary condition.

Figure 3(c) shows the output voltage across the optimal resistive load. Under constant temperature boundary condition (Figure 3(c-i)), voltage increases almost linearly with increase in FF and it is affected slightly by change in AR. On contrary, under constant heat flux boundary condition (Figure 3(c-ii)), output voltage increases with increases in both FF as well as AR. Figure 3(d) depicts variation in internal temperature difference ($T_h - T_c$) with change in FF and AR. Under constant temperature boundary condition (Figure 3(d-i)), hot-side and cold-side temperatures are fixed; therefore, temperature difference does not change. Under constant heat flux boundary condition (Figure 3(d-ii)), temperature difference increases slightly with increase in AR, but drastically with decreases in FF. It can be noted from equations (8)-(9) that TEG internal electrical (R_{eTEG}) and thermal (R_{tTEG}) resistances are directly proportional to AR and inversely proportional to FF. Under constant temperature boundary condition, small R_{eTEG} is desired as it causes less Joule heating. Therefore, in this case, large FF and small AR result in a better TEG performance. On the other hand, under constant heat flux condition, a large R_{tTEG} is desired, as it tends to produce large temperature difference ($T_h - T_c$). Therefore, in this condition, small FF and large AR is preferred. However, extremely large AR may result in extremely large R_{eTEG}, which negatively impacts TEG performance due to increased Joule heating. Therefore, TEGs under constant heat flux boundary condition require an optimized AR.

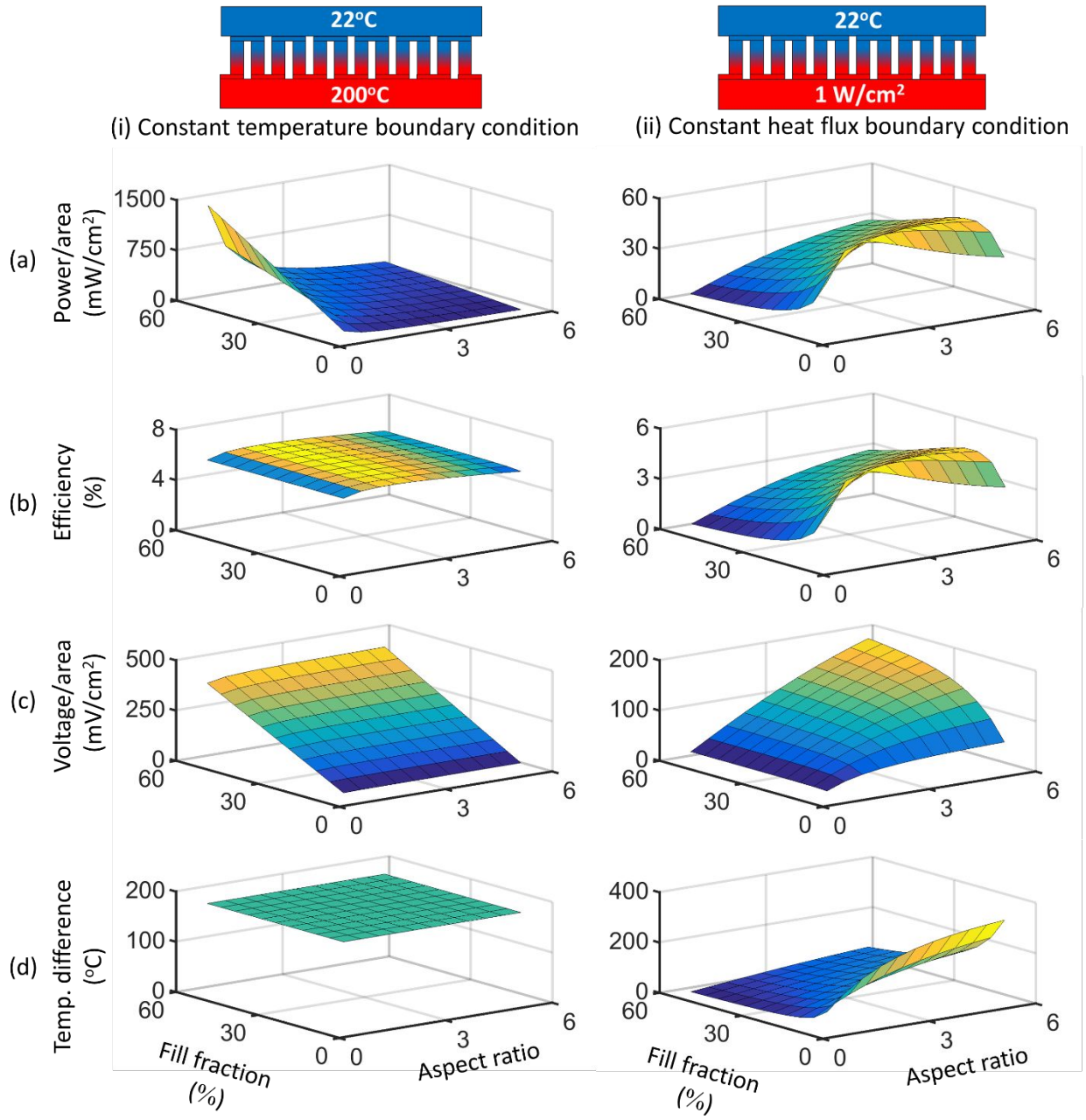

Figure 3. The effect of fill fraction (FF) and leg aspect ratio (AR) on TEG performance under two different boundary conditions. (a-i) Under constant temperature boundary condition, power increases linearly with increase in FF, whereas it decreases with increase in AR. (a-ii) Under constant heat flux boundary condition, power increases with decrease in FF and there exists an optimal AR where power is maximum. (b-i) Under constant temperature boundary condition, efficiency is largely unaffected by TEG design; however, large FF and AR close to 1.5 result in a highest efficiency. (b-ii) Under constant heat flux boundary condition, efficiency is high at low FF

and at an optimized AR. (c-i) Voltage across the optimal load increases almost linearly with increase in FF and is mostly unaffected by change in AR. (c-ii) Under constant heat flux boundary condition, voltage across the optimal load increases with increases in both FF as well as AR. (d-i) Under constant temperature boundary condition, temperature difference does not change with change in FF or AR. (d-ii) Under constant heat flux boundary condition, temperature difference temperature difference increases slightly with increase in AR, but it decreases drastically with increases in FF.

The effect of external thermal resistances on module design

The external thermal resistances, such as thermal resistance of heat source or heat sink, greatly influence the heat flow rate through the TEG and the hot-side and cold-side temperatures. Therefore, based upon the applications and thus the magnitude of external thermal resistances, TEG modules must be optimized to enhance its performance. Figure 4 and Figure 5 demonstrate the variation in TEG performance with change in heat source thermal resistance (R_{source}). R_{source} can be expressed as: $R_{source} = \frac{1}{hA}$, where A is the base area of TEG module and h is the heat transfer coefficient, whose value can vary based on the heat transfer medium used in the heat exchanger (see Supporting Information Table S1). When value of h is extremely large, the thermal resistance of heat source is very small, i.e. $R_{source} \approx 0$. This infers that hot-side temperature of TEG is nearly equal to the core temperature of heat source ($T_{source} = T_h$), which represents a constant temperature boundary condition. On the contrary, when value of h is extremely small, thermal resistance of heat source is very large. If $R_{source} \gg R_{tTEG}$, the heat flow through the TEG is almost unaffected by TEG operation; therefore, this case represents a constant low heat flux boundary condition.

Figure 4 shows TEG performance under the optimal load versus h at different FFs. Columns (i), (ii), and (iii) illustrate TEG performance at fixed AR of 0.5, 2.0, and 4.0, respectively. Figure 4(a) depicts TEG power versus h. It can be noted that when h is small (i.e. R_{source} is large), low FF results in high power, whereas when h is large (or R_{source} is small), large FF results in high power. It is quite interesting to note that there is a critical heat transfer coefficient (h_c) where TEG design drastically changes. When $h < h_c$, low FF is preferred; whereas, when $h > h_c$, large FF is required. Also, it can be noted that h_c decreases with increase in AR. When AR=0.5, $h_c > 100$ W/m^2-K;

when AR=2.0, $h_c \approx 100$ W/m^2-K; and when AR=0.5, $h_c < 100$ W/m^2-K. Figure 4(b) depicts TEG efficiency versus h. It can be observed that low FF typically results in high efficiency; however, as the value of h increases, the effect of FF on efficiency reduces and when h is very large, TEG efficiency is almost independent of FF. Figure 4(c) depicts TEG voltage across the optimal load. Clearly, high FF produces high voltage. Lastly, looking at Figure 4(d), it can be observed that low FF results in large temperature difference when h is small. When h is large, temperature difference is largely unaffected by change in FF.

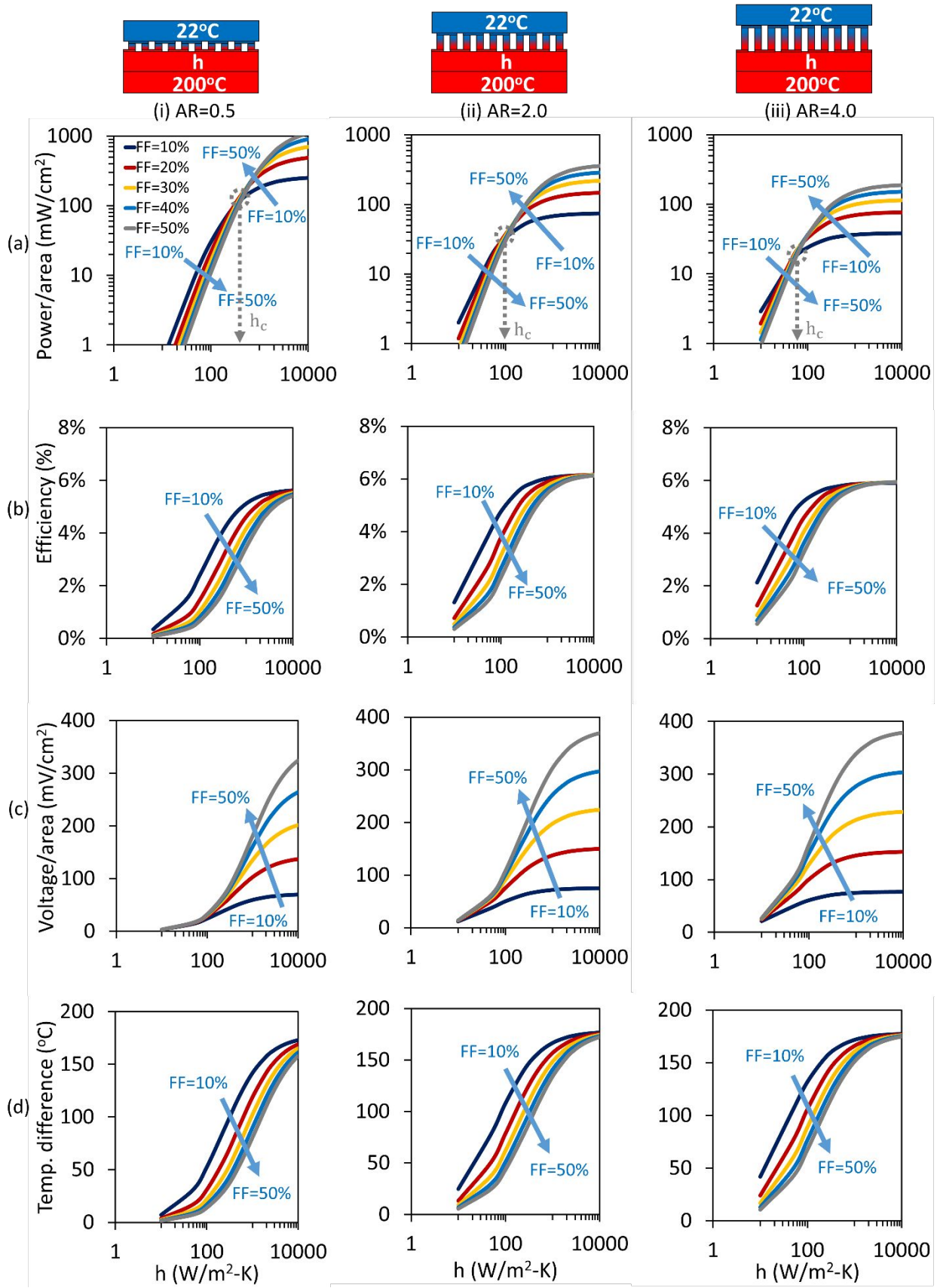
22°C
h
200°C
(i) AR=0.5
(ii) AR=2.0
(iii) AR=4.0
(a)
Power/area (mW/cm²)
FF=10%
FF=20%
FF=30%
FF=40%
FF=50%
FF=10%
FF=50%
h_c
(b)
Efficiency (%)
(c)
Voltage/area (mV/cm²)
(d)
Temp. difference (°C)
h (W/m²-K)

Figure 4. Effect of external thermal resistance on TEG design and performance. Plots illustrate the variation in TEG performance versus heat transfer coefficient (h) at different fill fractions (FFs). Column (i), (ii), and (iii) illustrate results for TEGs with leg AR of 0.5, 2.0, and 4.0, respectively. (a) TEG power versus h; when h is small (i.e. R_{source} is large), TEG requires low FF, whereas when h is large (or R_{source} is small), TEG requires large FF. There exists a critical heat transfer coefficient (h_c) where TEG design drastically changes. (b) TEG efficiency versus h. Typically, low FF results in high efficiency; however, when h is very large, TEG efficiency is independent of FF. (c) TEG voltage versus h. High FF generates higher voltage across the optimal load. (d) Temperature difference versus h. Low FF results in high temperature difference when h is in small to medium range. When h is large, temperature difference is largely unaffected by change in FF.

Figure 5(a) illustrates the TEG power versus h at different leg ARs. It can be noted that when h is small (i.e. R_{source} is large), large AR results in large power; however, when h is large (or R_{source} is small), small AR results in high power. Critical heat transfer coefficient (h_c) increases with increase in FF. When FF=10%, $h_c < 250$ W/m^2-K; when FF=25%, $h_c \approx 250$ W/m^2-K; and when FF=50%, $h_c > 250$ W/m^2-K. Figure 5(b) depicts TEG efficiency versus h. It can be observed that when h is in small to medium range, a large AR is desired; however, when h is very large, a nominal value of AR provides better efficiency. Looking at Figure 5(c) and (d), it can be observed that voltage and temperature difference follow similar trend and both these parameters are high when AR is large.

It is interesting to note from Figure 4 and Figure 5 that TEG design at the two extreme values of h (i.e. when h is very small, or h is very large) matches closely with the TEG design obtained for constant heat flux boundary condition and constant temperature boundary condition, respectively. This is expected as small value of h represents a low constant heat flux boundary condition, whereas large h signifies constant temperature boundary condition. This discussion also highlights that the commercial TEG modules that usually have large FF (> 25%) and low AR (1.0-1.5) are suitable for applications having small external thermal resistance. For the applications, where external thermal resistance is large, TEG modules with small FF and large AR are desired. This

observation is in agreement with the TEG design reported for wearable TE modules [44, 48]. Since human skin and ambient air have low thermal conductivity, wearable TEGs operate under the huge thermally resistive environment. For such applications, commercial TEG modules have been found to generate much lower power than the customized TEGs having small FF and large AR. Please note that the critical heat transfer coefficient is observed only for TEG power not for TEG efficiency. TEG efficiency cannot be higher than the theoretical limit. When h is small, TEG efficiency is greatly affected by FF and leg AR. However, when h becomes large, this condition approaches ideality, allowing TEG efficiency to approach the theoretical limit. TEG efficiency, under such condition, is nearly unaffected by TEG geometric parameters.

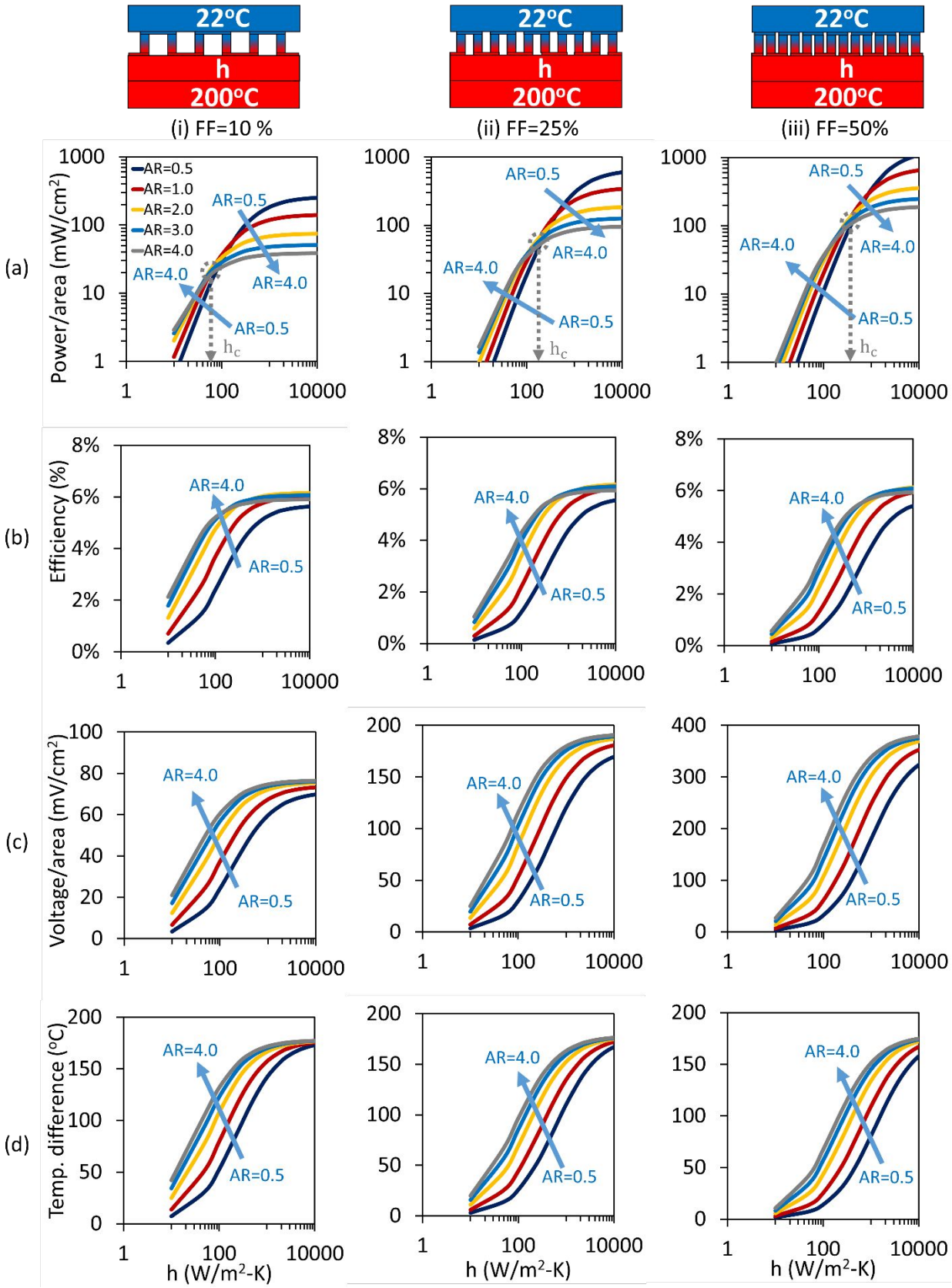
22°C
h
200°C
(i) FF=10 %
(ii) FF=25%
(iii) FF=50%
(a)
Power/area (mW/cm²)
AR=0.5
AR=1.0
AR=2.0
AR=3.0
AR=4.0
(b)
Efficiency (%)
(c)
Voltage/area (mV/cm²)
(d)
Temp. difference (°C)
h (W/m²-K)
h_c

Figure 5. Effect of external thermal resistance on TEG design at different leg aspect ratios (ARs). Column (i), (ii), and (iii) illustrate results for TEGs with fill fraction (FF) of 10%, 25% and 50%, respectively. (a) TEG power versus h. When h is small (i.e. R_{source} is large), TEG requires a large AR, whereas when h is large (or R_{source} is small), TEG requires a small AR. Critical heat transfer coefficient (h_c) increases with increase in FF. (b) TEG efficiency versus h. When h is in small to medium range, a large AR is desired; however, when h is extremely large, a nominal value of AR close to 1.5 provides a better efficiency. (c) TEG voltage versus h. Voltage across the optimal load increases with increase in AR for all values of h. (d) Temperature difference versus h. Temperature difference is high when AR is large.

Experimental

In order to validate the theoretical predictions, experiments were performed using TEG modules with different set of design parameters. Figure 6(a) and (b) illustrate TEG modules having same leg aspect ratio (AR=1.0) but different fill fraction (FF=12% and 36%). Figure 6(c) and (d) depict TEG modules having nearly same fill fraction (FF=24-27%) but different leg aspect ratio (AR=1.0 and 4.0). The TEG modules were characterized using the experimental set-up shown in Figure 6(e)-(g). Modules were placed between a heat source and heat sink (shown in Figure 6(e)). The hot-side temperature was maintained at 100°C using a heater, copper block and a temperature controller (feedback loop). The cold-side temperature was fixed at 16.5°C using a heat sink and a water chiller. Thermal resistors of known thermal conductivity, cross-sectional area and thickness were placed between the heat source and TEG to vary the heat transfer coefficient (Figure 6(f)). Thermal paste was used as the interface material and temperature was measured using a K-type thermocouple (Omega Engineering). The experiments were conducted in vacuum as well as in ambient air conditions using set-up shown in Figure 6(g). The more details about the fabrication and characterization of the TEG modules are presented elsewhere [61].

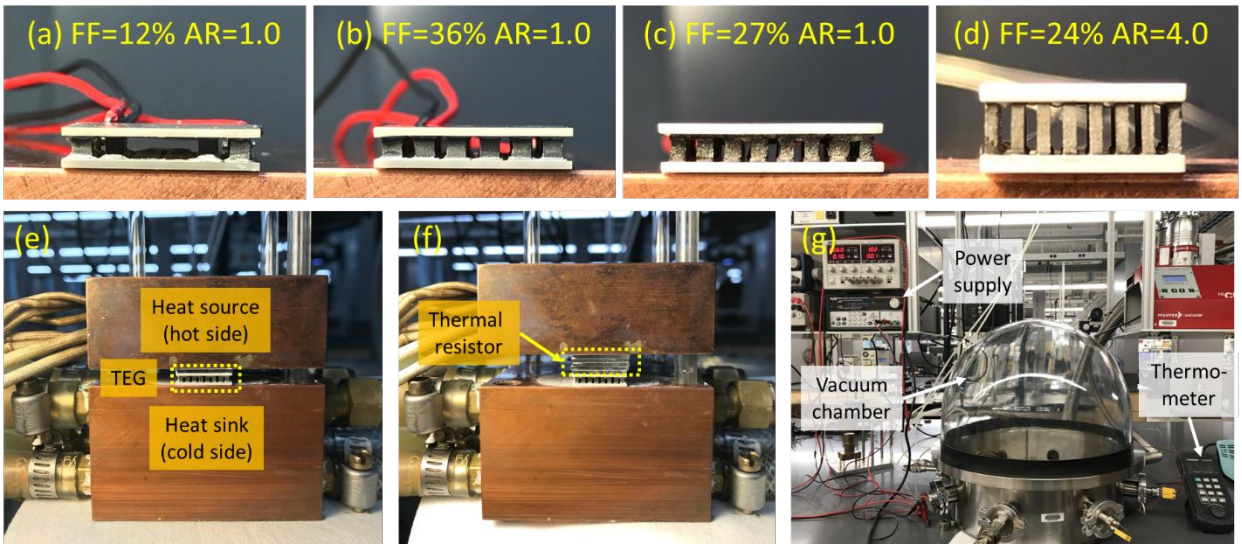

Figure 6. The TEG modules and set-up used for experimental validation. TEG modules with (a) FF=12% and leg AR=1.0, (b) FF=36% and leg AR=1.0, (c) FF=27% and leg AR=1.0, and (d) FF=24% and leg AR=4.0. Experimental set-up illustrating (e) heat source, heat sink, and TEG modules, (f) thermal resistors of known thermal conductivity and thickness to vary the heat transfer coefficient, and (g) vacuum chamber and measurement set-up.

Figure 7(a) and (c) compare the optimal power output from two TEGs having different FFs (FF=12% and FF=36%) but same leg AR (AR=1.0) in vacuum and in air, respectively. It can be clearly noted that, when external thermal resistance is small (i.e. h is large and greater than 250 W/m^2-K), the TEG with FF=36% generates higher power than the TEG with FF=12%. However, when external thermal resistance is large (h is small and less than 250 W/m^2-K), the TEG with smaller FF (FF=12%) results in higher power than the TEG with FF=36%. Figure 7(b) and (d) compare the optimal power output from two TEG modules having AR of 1.0 and 4.0 in vacuum and air, respectively. These modules have FF close to 25%. Although the effect of AR is not as pronounced as FF, it can be clearly noted that the TEG with AR=4.0 results in higher power than the TEG with AR=1.0, when h is small (< 650 W/m^2-K). The trend, however, changes as the value of h increases. When h > 650 W/m^2-K, the TEG with AR=1.0 generates higher power than the TEG with AR=4.0. These experiments clearly demonstrate the existence of a critical heat transfer coefficient that affects the design and performance of TEGs. It can also be noted in Figure 7 that TEG performance in vacuum and air seems nearly identical. Hot-side temperature for this

experiment is low (T_h=100°C); therefore, heat losses from TEG legs due to natural convection is negligible due to small temperature difference between TEG and ambient air. Consequently, critical heat transfer coefficient for TEG in air and TEG in vacuum is also same. The critical heat transfer coefficients in the two cases, however, can be different when hot-side temperature is high.

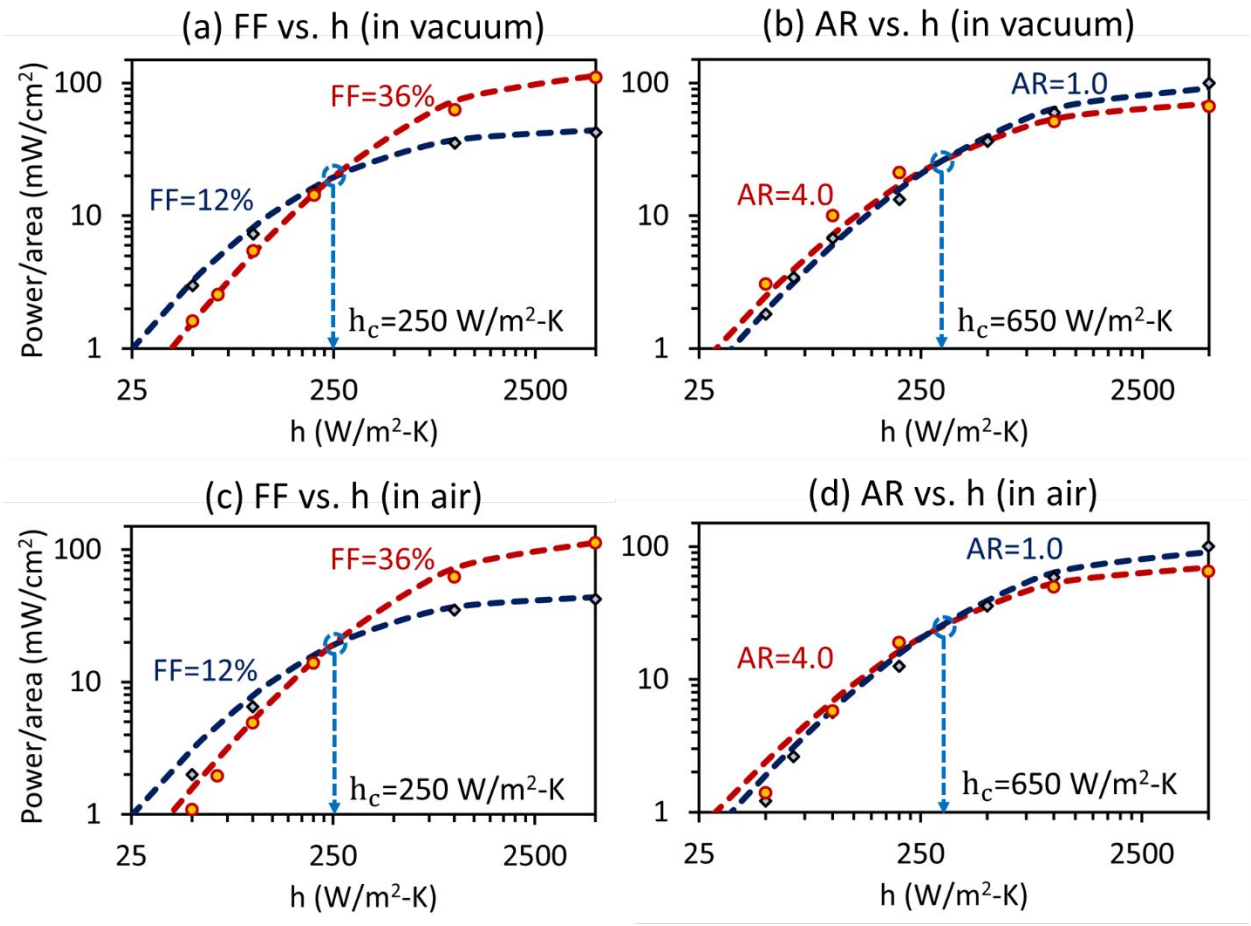

Figure 7. Experimental results validating theoretical prediction of the existence of critical heat transfer coefficient. Circles denote the experimental results and the dotted lines represent modeling results. (a)-(b) TEG power in vacuum condition. (c)-(d) TEG power in ambient air. (a) and (c) TEG with FF=36% generates higher power when h> 250 W/m^2-K; however, when h< 250 W/m^2-K TEG with FF=12% generates higher power. (b) and (d) TEG with AR=1.0 produces higher power when h> 650 W/m^2-K; however, when h< 650 W/m^2-K, TEG with AR=4.0 generates higher power.

Experimental Demonstration of Waste Heat Recovery from Hot-Water Pipe

Figure 8(a) shows a practical demonstration where TEG module is deployed on a hot-water pipe for low-grade waste heat recovery. Temperature of the water pipe was varied in the range of 35-50°C, while ambient condition was fixed at ~22°C with negligible air flow. Thermal paste was used as the interface material between the water pipe and the TEG to minimize the thermal loss at junction. The TEG modules were held for 20 min on the hot-water pipe to attain the steady state condition before measurements were recorded. Figure 8(b) and (c) compare the power generation from various custom-built TEG modules with the performance of a commercial module (part # 03111-5L31-03CF by Custom Thermoelectric Inc.). Various custom-built modules with FF varying from 1.7% to 36% were fabricated to study the effect of FF fraction on waste heat recovery compared to the commercial TEG module with FF of 28%. Table S2 in Supporting Information provides detailed information about our TEG modules.

TEGs deployed on the hot-water pipe operate under large external thermal resistance, particularly due to low thermal conductivity of ambient air ($\kappa_{air} \approx$ 0.025 W/m-K). As predicted by numerical calculations, the performance of commercial TEG is lower than that of the custom-built modules with optimized FF. It was noted that while temperature of the hot-water pipe remained the same, the temperature difference ($T_h - T_c$) across the two-sides of TEG modules was higher for TEG with lower FF. For instance, when hot-water pipe temperature was 35°C, temperature difference of 3.6°C was observed across the TEG with FF=12% while temperature difference of 2.7°C was observed across the TEG with FF=36%. Along similar lines, when hot-water pipe temperature was 50°C, temperature difference of 8.9°C and 4.8°C was noted for the TEGs with FF of 12% and 36%, respectively. Lower FF provides higher thermal resistance of the TEG module, that results in higher temperature difference. Therefore, low FF favors high power generation from TEG. However, when the FF is very low, electrical resistance dominates and results in reduction in the TEG power. It can be noted from Figure 8(c) that the TEG with FF=12% has the highest power. The commercial TEG generates 60.1 μW/cm^2 when the pipe temperature is 35°C and 301.8 μW/cm^2 when the pipe temperature is 50°C. On the other hand, the TEG with FF=12%, generates 65.5 μW/cm^2 when the pipe temperature is 35°C and 386.7 μW/cm^2 when the pipe temperature is 50°C. Thus, 12% FF TEG design presented in this paper provides 10% higher power than that of the commercial module at 35°C and 28% higher power than the commercial module at 50°C. It is

important to note that low FF TEG utilizes less materials; therefore, power over mass of TE materials is higher for the lower FF TEG than the higher FF TEG. This is important particularly for the applications where weight of the device is crucial. In addition to performance, the amount of TE materials used in a TEG module has direct impact on the module cost. Therefore, in Figure 8(d), we have compared power per unit mass of TE materials for different TEGs. Clearly, TEG power over mass of TE materials increases dramatically with decrease in FF. Comparing against the commercial module, our TEG with FF=12% utilizes 180% lesser TE materials. Therefore, power per unit mass of TE materials for the TEG with FF=12% is found to be 123% higher at 35°C and 162% higher at 50°C as compared to the commercial TEG. This demonstration clearly emphasizes that high FF commercial modules are not the optimal design for waste heat recovery.

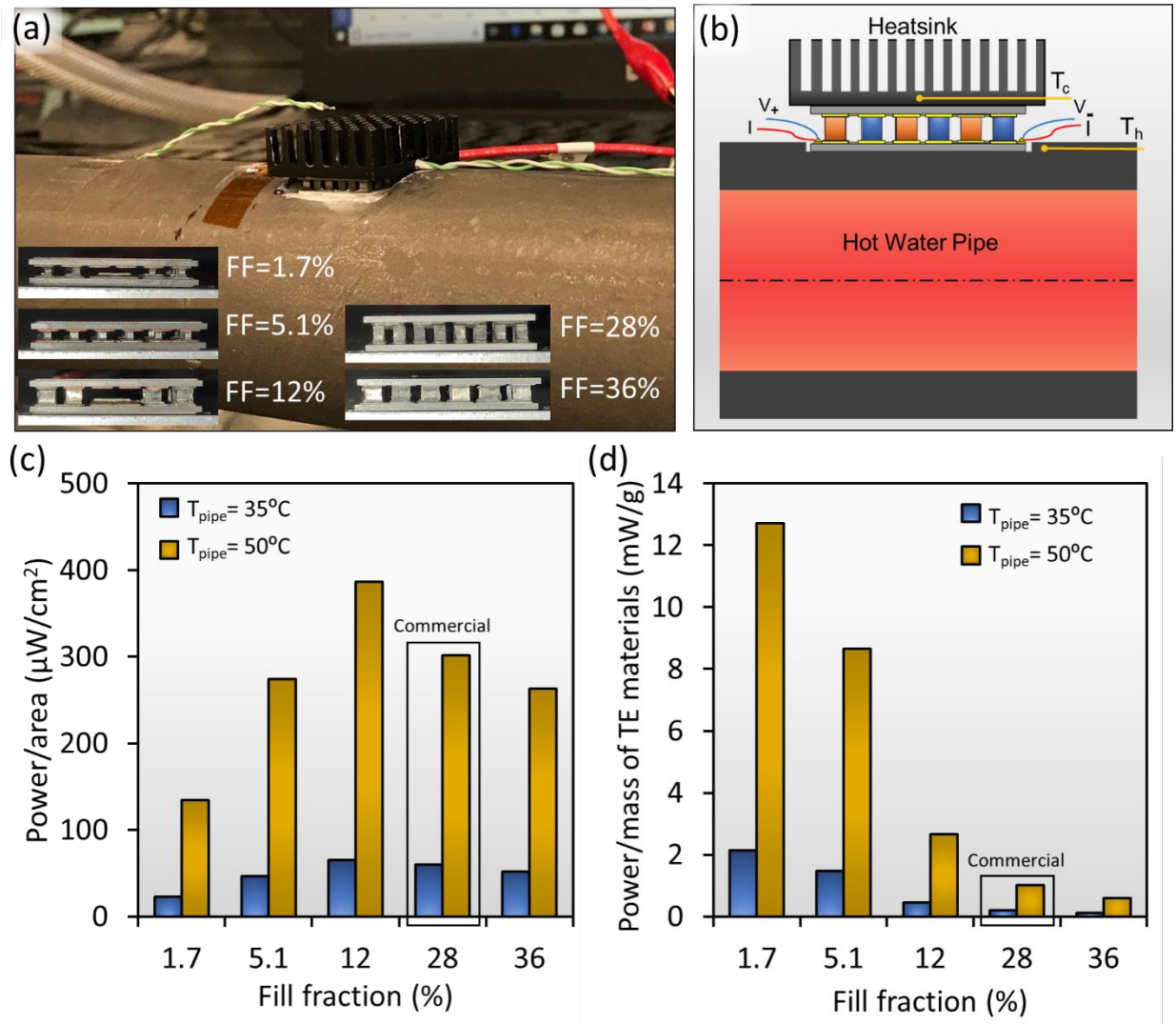

Figure 8. A practical demonstration for low-grade waste heat recovery using TEG modules. (a) Picture of the prototype and TEG modules used for demonstration, (b) Schematic representation of TEG module deployed on a hot-water pipe. Temperature of the hot-water pipe, T_{pipe} = 35-50°C and ambient temperature T_{amb}=22 °C. (c) Power over TEG base area for TEGs with FF=1.7%, 5.1%, 12%, 28% (commercial) and 36%. (d) Power density (power over mass of TE materials) for different custom-built TEGs versus the commercial TEG.

Conclusions

This study demonstrated that the deployment environments, particularly boundary conditions and external thermal resistances, strongly influence the TE materials behavior, TEG design and TEG performance. It was noted that performance of a TEG under constant heat flux condition is drastically different than its behavior under the constant temperature boundary condition. Under constant temperature boundary condition, large Seebeck coefficient and higher zT result in better TEG performance. However, under constant heat flux boundary condition, low thermal conductivity results in superior TEG performance. The boundary conditions were found to have significant effect on TEG design. When a constant temperature boundary condition is maintained, high FF and small AR are required for the optimal TEG performance. However, under constant heat flux boundary condition, low FF and an optimal leg AR is shown to provide superior TEG performance. TEG design and performance were found to vary with variation in the external thermal resistances. When external thermal resistance is small, TEG requires large FF and AR close to 1.5. When external thermal resistance is large, TEG requires low FF and an optimized leg AR. A critical heat transfer coefficient was identified where TEG design drastically changes. For low-grade waste heat recovery from the hot-water pipe, the optimized TEG (FF=12% and AR=1.0) generated 28% higher power and 162% higher power per unit mass of TE materials as compared to the commercial modules.

Table of Contents (TOC) graphic

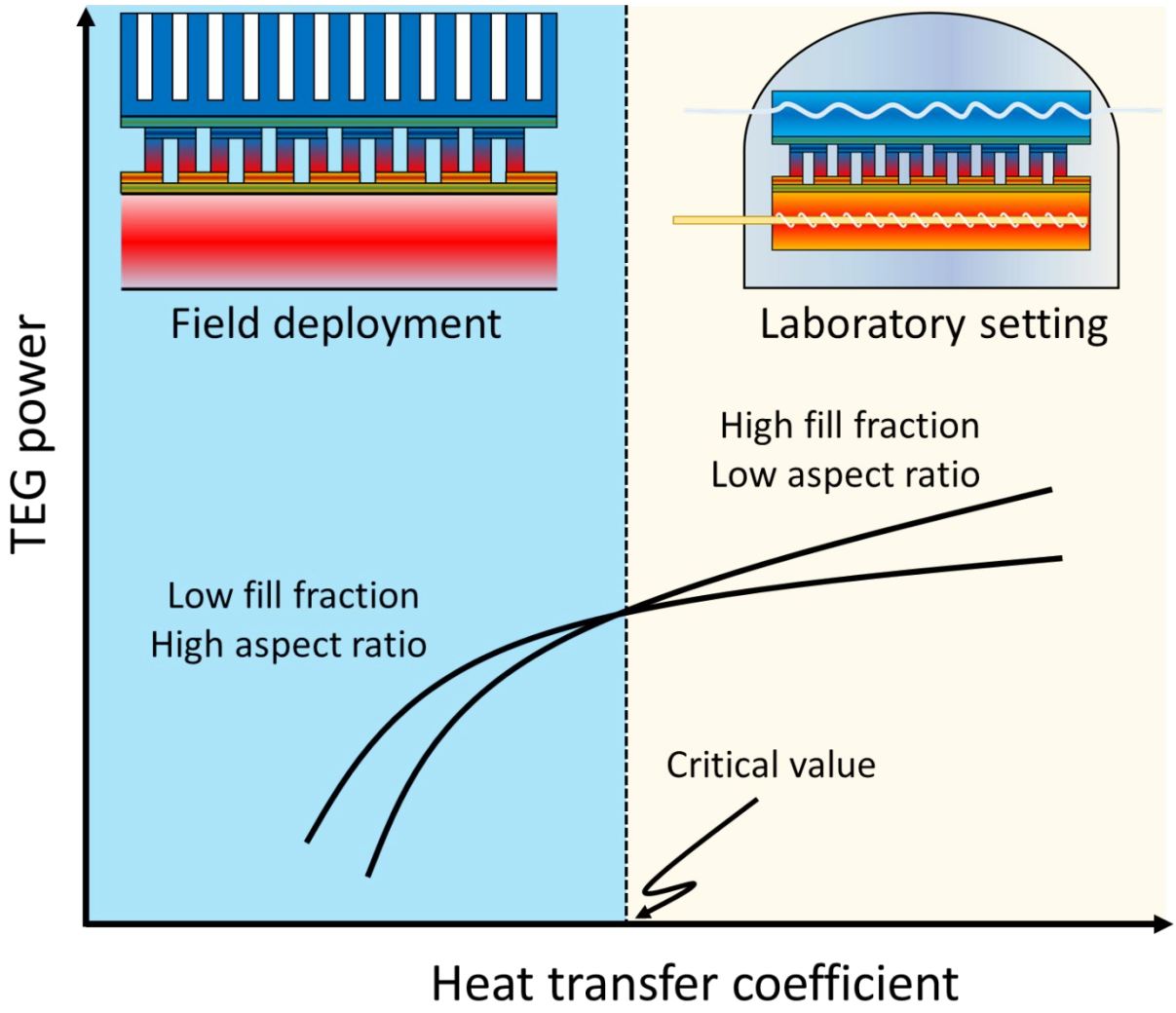

Author contributions: R.A.K., A.N., and B.P. conceived the idea; R.A.K. performed modeling, A.N. and B.P. fabricated modules and performed the experiments; S.P. supervised the overall research. All authors contributed to the discussions and writing of the manuscript.

Notes: The authors declare no competing financial interest.

Supporting information: Thermoelectric models, temperature-dependent thermoelectric material properties, typical values of heat transfer coefficient, and details of the TEG modules used for waste-heat recovery experiment

Acknowledgements: R.A.K. and S.P. acknowledge the financial support from DARPA TE3 program. A.N. and B.P. acknowledge the financial support from DARPA NETS program.

References

(1) Zhang, Q.; Liao, J.; Tang, Y.; Gu, M.; Ming, C.; Qiu, P.; Bai, S.; Shi, X.; Uher, C.; Chen, L. Realizing a thermoelectric conversion efficiency of 12% in bismuth telluride/skutterudite segmented modules through full-parameter optimization and energy-loss minimized integration. *Energy & Environmental Science* **2017,** *10* (4), 956-963.
(2) Shi, X.; Chen, L. Thermoelectric materials step up. *Nature materials* **2016,** *15* (7), 691–692.
(3) Anant Kishore, R.; Kumar, P.; Sanghadasa, M.; Priya, S. Taguchi optimization of Bismuth-Telluride based thermoelectric cooler. *Journal of Applied Physics* **2017,** *122* (2), 025109.
(4) Minnich, A.; Dresselhaus, M.; Ren, Z.; Chen, G. Bulk nanostructured thermoelectric materials: current research and future prospects. *Energy & Environmental Science* **2009,** *2* (5), 466-479.
(5) Rowe, D. M. *CRC handbook of thermoelectrics*, CRC press: 1995.
(6) Snyder, G. J.; Toberer, E. S. Complex thermoelectric materials. *Nature Materials* **2008,** *7*, 105-114, DOI: 10.1038/nmat2090.
(7) Bell, L. E. Cooling, heating, generating power, and recovering waste heat with thermoelectric systems. *Science* **2008,** *321* (5895), 1457-1461.
(8) Baranowski, L. L.; Snyder, G. J.; Toberer, E. S. Concentrated solar thermoelectric generators. *Energy & Environmental Science* **2012,** *5* (10), 9055-9067.
(9) Stratistics-MRC. *Thermoelectric Generator - Global Market Outlook (2016-2022): https://www.strategymrc.com/report/thermoelectric-generator-market. Accessed on Nov 08, 2018.*
(10) Takahashi, K.; Kanno, T.; Sakai, A.; Tamaki, H.; Kusada, H.; Yamada, Y. Bifunctional thermoelectric tube made of tilted multilayer material as an alternative to standard heat exchangers. *Scientific reports* **2013,** *3*, 1501.
(11) Zebarjadi, M.; Esfarjani, K.; Dresselhaus, M.; Ren, Z.; Chen, G. Perspectives on thermoelectrics: from fundamentals to device applications. *Energy & Environmental Science* **2012,** *5* (1), 5147-5162.
(12) Tuley, R.; Placha, K.; Robbins, M.; Gilchrist, B.; Simpson, K. Automotive Power Harvesting/Thermoelectric Applications. In *Thermoelectric Materials and Devices*; 2016; pp 230-251.
(13) Schierning, G. Bring on the heat. *Nature Energy* **2018,** *3*, 92-93.
(14) Kishore, R. A.; Kumar, P.; Priya, S. A comprehensive optimization study on Bi 2 Te 3-based thermoelectric generators using the Taguchi method. *Sustainable Energy & Fuels* **2018,** *2* (1), 175-190.
(15) Bahk, J.-H.; Fang, H.; Yazawa, K.; Shakouri, A. Flexible thermoelectric materials and device optimization for wearable energy harvesting. *Journal of Materials Chemistry C* **2015,** *3* (40), 10362-10374.
(16) Du, Y.; Cai, K.; Chen, S.; Wang, H.; Shen, S. Z.; Donelson, R.; Lin, T. Thermoelectric fabrics: toward power generating clothing. *Scientific reports* **2015,** *5*, 6411.

(17) Ito, M.; Koizumi, T.; Kojima, H.; Saito, T.; Nakamura, M. From materials to device design of a thermoelectric fabric for wearable energy harvesters. *Journal of Materials Chemistry A* **2017,** *5* (24), 12068-12072.
(18) Chen, T.; Guai, G. H.; Gong, C.; Hu, W.; Zhu, J.; Yang, H.; Yan, Q.; Li, C. M. Thermoelectric Bi 2 Te 3-improved charge collection for high-performance dye-sensitized solar cells. *Energy & Environmental Science* **2012,** *5* (4), 6294-6298.
(19) Sundarraj, P.; Maity, D.; Roy, S. S.; Taylor, R. A. Recent advances in thermoelectric materials and solar thermoelectric generators–a critical review. *RSC Advances* **2014,** *4* (87), 46860-46874.
(20) Shi, B.; Su, H.; Li, J.; Qi, H.; Zhou, F.; Torero, J. L.; Chen, Z. Clean power generation from the intractable natural coalfield fires: Turn harm into benefit. *Scientific reports* **2017,** *7* (1), 5302.
(21) Vining, C. B. An inconvenient truth about thermoelectrics. *Nature materials* **2009,** *8* (2), 83-85.
(22) Kishore, R. A.; Sanghadasa, M.; Priya, S. Optimization of segmented thermoelectric generator using Taguchi and ANOVA techniques. *Scientific reports* **2017,** *7* (1), 16746.
(23) Snyder, G. J.; Snyder, A. H. Figure of merit ZT of a thermoelectric device defined from materials properties. *Energy & Environmental Science* **2017,** *10* (11), 2280-2283.
(24) Kim, H. S.; Liu, W.; Ren, Z. The bridge between the materials and devices of thermoelectric power generators. *Energy & Environmental Science* **2017,** *10* (1), 69-85.
(25) LeBlanc, S. A. Electrothermal Properties of Nanowire Materials for Energy Conversion Systems. Stanford University A Dissertation Submitted to the Department of Mechanical Engineering, 2012.
(26) LeBlanc, S. Thermoelectric generators: Linking material properties and systems engineering for waste heat recovery applications. *Sustainable Materials and Technologies* **2014,** *1*, 26-35.
(27) Yazawa, K.; Shakouri, A. Optimization of power and efficiency of thermoelectric devices with asymmetric thermal contacts. *Journal of Applied Physics* **2012,** *111* (2), 024509.
(28) Mayer, P.; Ram, R. Optimization of heat sink–limited thermoelectric generators. *Nanoscale and Microscale Thermophysical Engineering* **2006,** *10* (2), 143-155.
(29) Chen, L.; Gong, J.; Sun, F.; Wu, C. Effect of heat transfer on the performance of thermoelectric generators. *International journal of thermal sciences* **2002,** *41* (1), 95-99.
(30) Kishore, R. A.; Mahajan, R. L.; Priya, S. Combinatory finite element and artificial neural network model for predicting performance of thermoelectric generator. *Energies* **2018,** *11* (9), 2216.
(31) Kishore, R. A.; Priya, S. A review on low-grade thermal energy harvesting: materials, methods and devices. *Materials* **2018,** *11* (8), 1433.
(32) Dunham, M. T.; Barako, M. T.; LeBlanc, S.; Asheghi, M.; Chen, B.; Goodson, K. E. Power density optimization for micro thermoelectric generators. *Energy* **2015,** *93*, 2006-2017.
(33) Yang, R.; Chen, G.; Snyder, G. J.; Fleurial, J.-P. Multistage thermoelectric microcoolers. *Journal of applied physics* **2004,** *95* (12), 8226-8232.
(34) Yilbas, B.; Sahin, A. Thermoelectric device and optimum external load parameter and slenderness ratio. *Energy* **2010,** *35* (12), 5380-5384.
(35) Sahin, A. Z.; Yilbas, B. S. The thermoelement as thermoelectric power generator: effect of leg geometry on the efficiency and power generation. *Energy Conversion and Management* **2013,** *65*, 26-32.
(36) Rowe, D.; Min, G. Design theory of thermoelectric modules for electrical power generation. *IEE Proceedings-Science, Measurement and Technology* **1996,** *143* (6), 351-356.
(37) Mitrani, D.; Salazar, J.; Turó, A.; García, M. J.; Chávez, J. A. One-dimensional modeling of TE devices considering temperature-dependent parameters using SPICE. *Microelectronics Journal* **2009,** *40* (9), 1398-1405.
(38) Wang, X.-D.; Huang, Y.-X.; Cheng, C.-H.; Lin, D. T.-W.; Kang, C.-H. A three-dimensional numerical modeling of thermoelectric device with consideration of coupling of temperature field and electric potential field. *Energy* **2012,** *47* (1), 488-497.

(39) Pérez–Aparicio, J.; Palma, R.; Taylor, R. Finite element analysis and material sensitivity of Peltier thermoelectric cells coolers. *International Journal of Heat and Mass Transfer* **2012,** *55* (4), 1363-1374.
(40) Cheng, C.-H.; Huang, S.-Y.; Cheng, T.-C. A three-dimensional theoretical model for predicting transient thermal behavior of thermoelectric coolers. *International Journal of Heat and Mass Transfer* **2010,** *53* (9), 2001-2011.
(41) Meng, J.-H.; Wang, X.-D.; Zhang, X.-X. Transient modeling and dynamic characteristics of thermoelectric cooler. *Applied energy* **2013,** *108*, 340-348.
(42) Zaitsev, V.; Fedorov, M.; Eremin, I.; Gurieva, E.; Rowe, D. Thermoelectrics handbook: macro to nano. *CRC Press, Taylor & Francis, Boca Raton* **2006**.
(43) Zhao, D.; Tan, G. A review of thermoelectric cooling: materials, modeling and applications. *Applied Thermal Engineering* **2014,** *66* (1-2), 15-24.
(44) Kishore, R. A.; Nozariasbmarz, A.; Poudel, B.; Sanghadasa, M.; Priya, S. Ultra-high performance wearable thermoelectric coolers with less materials. *Nature communications* **2019,** *10* (1), 1765.
(45) Ouyang, Z.; Li, D. Modelling of segmented high-performance thermoelectric generators with effects of thermal radiation, electrical and thermal contact resistances. *Scientific reports* **2016,** *6* (1), 1-12.
(46) Stobart, R.; Yang, Z.; Lan, S. System design considerations for thermoelectric energy recovery. *Thermoelectric Materials and Devices* **2016,** (17), 156-203.
(47) Crane, D. T.; Jackson, G. S. In *Systems-level optimization of low-temperature thermoelectric waste heat recovery*, 2002; IEEE: pp 583-591.
(48) Suarez, F.; Nozariasbmarz, A.; Vashaee, D.; Öztürk, M. C. Designing thermoelectric generators for self-powered wearable electronics. *Energy & Environmental Science* **2016,** *9* (6), 2099-2113.
(49) Nozariasbmarz, A.; Collins, H.; Dsouza, K.; Polash, M. H.; Hosseini, M.; Hyland, M.; Liu, J.; Malhotra, A.; Ortiz, F. M.; Mohaddes, F. Review of wearable thermoelectric energy harvesting: From body temperature to electronic systems. *Applied Energy* **2019**, 114069.
(50) Leonov, V.; Vullers, R. J. M. Wearable thermoelectric generators for body-powered devices. *Journal of electronic materials* **2009,** *38* (7), 1491-1498.
(51) Nozariasbmarz, A.; Suarez, F.; Dycus, J. H.; Cabral, M. J.; LeBeau, J. M.; Öztürk, M. C.; Vashaee, D. Thermoelectric generators for wearable body heat harvesting: Material and device concurrent optimization. *Nano Energy* **2020,** *67*, 104265.
(52) Yee, S. K.; LeBlanc, S.; Goodson, K. E.; Dames, C. $ per W metrics for thermoelectric power generation: beyond ZT. *Energy & Environmental Science* **2013,** *6* (9), 2561-2571.
(53) Mayer, P. M.; Ram, R. J. Optimization of heat sink–limited thermoelectric generators. *Nanoscale and Microscale Thermophysical Engineering* **2006,** *10* (2), 143-155.
(54) Suzuki, R. O.; Fujisaka, T.; Ito, K. O.; Meng, X.; Sui, H.-T. Dimensional analysis of thermoelectric modules under constant heat flux. *Journal of electronic materials* **2015,** *44* (1), 348-355.
(55) Shen, Z.-G.; Wu, S.-Y.; Xiao, L. Assessment of the performance of annular thermoelectric couples under constant heat flux condition. *Energy Conversion and Management* **2017,** *150*, 704-713.
(56) Chen, G. Theoretical efficiency of solar thermoelectric energy generators. *Journal of Applied Physics* **2011,** *109* (10), 104908.
(57) Deng, R.; Su, X.; Hao, S.; Zheng, Z.; Zhang, M.; Xie, H.; Liu, W.; Yan, Y.; Wolverton, C.; Uher, C. High thermoelectric performance in Bi 0.46 Sb 1.54 Te 3 nanostructured with ZnTe. *Energy & Environmental Science* **2018,** *11*, 1520-1535.
(58) Hao, F.; Qiu, P.; Tang, Y.; Bai, S.; Xing, T.; Chu, H.-S.; Zhang, Q.; Lu, P.; Zhang, T.; Ren, D. High efficiency Bi 2 Te 3-based materials and devices for thermoelectric power generation between 100 and 300 C. *Energy & Environmental Science* **2016,** *9* (10), 3120-3127.
(59) Zhao, L.-D.; Dravid, V. P.; Kanatzidis, M. G. The panoscopic approach to high performance thermoelectrics. *Energy & Environmental Science* **2014,** *7* (1), 251-268.

(60) Ouyang, Z.; Li, D. Modelling of segmented high-performance thermoelectric generators with effects of thermal radiation, electrical and thermal contact resistances. *Scientific reports* **2016,** *6*, 24123.
(61) Nozariasbmarz, A.; Kishore, R. A.; Poudel, B.; Saparamadu, U.; Li, W.; Cruz, R.; Priya, S. High Power Density Body Heat Energy Harvesting. *ACS Applied Materials & Interfaces* **2019,** *11* (43), 40107-40113.